Solar Energy 141 (2016): 236–241

DOI: http://doi.org/10.1016/j.solener.2016.11.035

Cu_2ZnSnS_4 thin film solar cells grown by fast thermal evaporation and thermal treatment

E. Garcia-Llamas[a], J.M. Merino[a], R. Gunder[b], K. Neldner[b], D. Greiner[b], A. Steigert[b], S. Giraldo[c], V. Izquierdo-Roca[c], E. Saucedo[c], M. León[a], S. Schorr[b,d], R. Caballero[a]*

[a]Universidad Autónoma de Madrid, Departamento de Física Aplicada, C/ Francisco Tomás y Valiente 7, 28049 Madrid, Spain
[b]Helmholtz Zentrum Berlin für Materialien und Energie, Hahn Meitner Platz 1, 14109 Berlin, Germany
[c]IREC, Catalonia Institute for Energy Research, C/ Jardins de les Dones de Negre 1, Sant Adriá del Besòs, 08930 Barcelona, Spain
[d]Freie Universitaet Berlin, Institute of Geological Sciences, Malteserstr. 74-100, 12249 Berlin, Germany

* Corresponding author: raquel.caballero@uam.es

Cu_2ZnSnS_4 thin films have been produced via rapid thermal evaporation of off-stoichiometric kesterite powder followed by annealing in an Ar atmosphere. Different heating rates were applied during the thermal treatments. The chemical composition and structural properties of the deposited layers as well as the distribution of the elements through the kesterite thin film have been investigated. The initial growth of a SnS secondary phase during evaporation led to the formation of this secondary phase next to the Mo back contact. Solar cell power conversion efficiencies were limited to values about 3 % due to this secondary phase. Furthermore, an increased open circuit voltage was demonstrated by using a Zn(O,S) buffer layer.

Keywords: kesterite solar cells; thin films; thermal evaporation; Zn(O,S) buffer layer

1. Introduction

Cu_2ZnSnS_4 (CZTS), $Cu_2ZnSnSe_4$ (CZTSe) and $Cu_2ZnSn(S,Se)_4$ (CZTSSe) kesterite materials are promising alternatives to $Cu(In,Ga)Se_2$ for photovoltaic applications. These materials are characterized by a high absorption coefficient and direct band gap energy in the range of 1.0 to 1.5 eV. Additionally, these kesterite materials are composed by low cost and abundant elements relative to indium [1]. Despite these properties, a maximum power conversion efficiency of 12.6 % has been achieved for CZTSSe devices [2], which is notably below the 22.6 % achieved for $Cu(In,Ga)Se_2$ solar cells [3].
The main limitation of kesterite solar cells is the open circuit voltage (V_{oc}) deficit relative to the absorber band gap energy (E_g) [4]. Different reasons for the large V_{oc} deficit (around 840 mV for CZTS) have been proposed. One reason that can explain the reduced V_{oc} is an unfavorable alignment of the conduction band minimum (CBM) at the CZTS/CdS interface. CdS has a lower CBM compared to CZTS, resulting in a "cliff" type of interface, which will lead to enhanced interface recombination. The use of $Zn_{1-x}Cd_xO_y$ buffer layer deposited by atomic layer deposition (ALD) instead of CdS has led to an increased in V_{oc} and device performance [5]. Another reason for the large V_{oc} deficit can be the non-optimal bulk quality of the kesterite absorber and the presence of secondary phases [6], such as SnS with lower E_g [7]. A Cu-poor / Zn-rich composition

seems to be ideal to achieve high performance CZTSSe devices [8]. This off-stoichiometry can result in the formation of ZnS(Se) secondary phase, which can block the current flow and introduce dead areas in the cell [6]. Moreover, the existence of large spatial band gap fluctuations coming from high concentrations of Cu-Zn antisite disorder can also contribute to the V_{oc} deficit [9]. The formation energy of defects is determined not only by the composition, but also by the growth parameters (temperature and pressure) of the absorber layer [4]. Variations in processing conditions affect the kesterite phase formation, and hence the solar cell devices performance. Many processing conditions and methods have been reported to grow quality kesterite films. CZTSSe solar cells fabricated by a hydrazine-based non-vacuum process exhibit a maximum power conversion efficiency of 12.6 % [2]. Alternatively, 9.1 % was achieved for a pure CZTS absorber layer fabricated by annealing of a glass/Mo/ZnS/Sn/Cu/ZnS precursor stack in H_2S balanced with N_2 [10-11]. Chemical routes have the advantage of reducing processing costs of the technology and have produced the best kesterite solar cells this far. Generally, vacuum-growth processes can lead to higher reproducibility and high quality semiconductor materials; however a higher processing cost is typically required.

The objective of this work is to grow quality CZTS thin films for efficient solar cells by fast evaporation technique. CZTS layers have been deposited by thermal evaporation of off-stoichiometric CZTS in only 12 minutes followed by annealing in Ar atmosphere, considerably reducing the synthesis time of kesterites. Up to our knowledge, this is the first time that kesterite thin film solar cells are produced by fast evaporation of the absorber layer. The effect of the heating rate in the thermal treatment on the properties of the kesterite absorber and solar cell devices is investigated. In addition, an attempt to increase V_{oc} was carried out by the use of a Zn(O,S) alternative buffer layer.

2. Experimental details

2.1. Deposition of Cu_2ZnSnS_4 thin films

For the evaporation source, a Cu-rich / S-poor Cu_2ZnSnS_4 compound was synthesized by solid state reaction [12]. CZTS thin films were fabricated by a two-stage process. In the first stage, CZTS thin films were deposited by thermal evaporation onto Mo coated glass using the precursor compound in powder form. CZTS powder was placed in a molybdenum crucible. The deposition rate was controlled by gradually increasing the current through the crucible, avoiding any spitting effect, and was monitored by a quartz crystal balance. Substrates were heated to nominal temperature of 250º C. CZTS thin films with a thickness of 1.5 μm were evaporated in only 12 minutes. The second stage of the process consisted of a thermal treatment of the samples at 550º C in Ar atmosphere at a pressure of 9.5×10^4 Pa under excess sulfur. For that purpose, the as-evaporated thin films were placed in a partially closed graphite box of 56 mm x 70 mm x 20.5 mm with a hole of 1 mm diameter in the lid, and inserted into a quartz tube furnace [13]. In order to have an overpressure of sulfur, 120 mg of pure elemental sulfur (99.999 %) were added to the graphite container. Heating rates of 2º C/min, 5ºC/min, 10ºC/min were used with cooling rate of 10º C/min in all cases. TT1, TT2 and TT3 refers to the thermal treatment with heating rates of 2º C/min, 5º C/min and 10º C/min, respectively. Here, the influence of the heating rate on the CZTS thin film properties was investigated. Table 1 summarizes the different thermal treatments carried out and the composition of the thin films and bulk compound.

Table 1. Thermal treatments and composition of the bulk and thin films.

Sample	Thermal treatment	Cu (at %)	Zn (at %)	Sn (at %)	S (at %)	Cu/(Zn+Sn)	Zn/Sn	S/M
Precursor	-	27.27	14.39	15.81	42.53	0.90	0.91	0.74
As-evap.	-	28.85	13.54	14.37	43.25	1.03	0.94	0.76
R7_TT1	2º C/min	20.68	11.84	16.08	51.40	0.74	0.74	1.06
	2º C/min + $(NH_4)_2S$	21.12	12.38	14.31	52.19	0.79	0.87	1.09
R7_TT2	5º C/min	20.82	11.71	16.19	51.29	0.75	0.72	1.05
	5º C/min + $(NH_4)_2S$	22.51	12.79	14.71	49.99	0.82	0.87	1.00
R7_TT3	10º C/min	20.82	11.33	15.35	52.5	0.78	0.74	1.11
	10º C/min + $(NH_4)_2S$	22.21	12.14	14.68	50.97	0.83	0.83	1.04

Note: All the thermal treatments were carried out at 550° C for 1 h.

2.2. Device fabrication

Solar cells with the CZTS absorber layers annealed at different heating rates were fabricated by using a CdS buffer layer deposited by chemical bath deposition. Two types of window layers were employed. In the first case, 50 nm of i-ZnO and 350 nm of In_2O_3:SnO_2 (ITO) were deposited by DC-pulsed sputtering to act as a transparent conductive window layer. In this case, the absorber layer was etched with $(NH_4)_2S$ before the buffer layer deposition [7]. In the second configuration, the window layer consisted of an i-ZnO/ZnO:Al (AZO) bilayer deposited by sputter deposition and Ni-Al grids were grown by thermal evaporation to enhance the current collection. In this last configuration, KCN etching was carried out before CdS deposition with the objective of cleaning the absorber surface and removing the possible oxides formed [14]. Moreover, an alternative buffer layer of Zn(O,S) was deposited by RF-sputtering, being the structure of the solar cell: glass/Mo/CZTS/Zn(O,S)/ZnO:Al/Ni-Al [15]. KCN etching was also performed before this alternative buffer layer. Table 2 shows photovoltaic parameters for solar cells fabricated from the described configurations.

Table 2. Photovoltaic parameters of the different CZTS solar cell devices.

Sample	Etching	Buffer	Window	V_{oc} (mV)	J_{sc} (mA/cm^2)	FF (%)	η (%)
R7_TT1	$(NH_4)_2S$	CdS	i-ZnO/ITO	551	10.7	36.9	2.2
R7_TT2	$(NH_4)_2S$	CdS	i-ZnO/ITO	336	11.2	33.3	1.3
	KCN	Zn(O,S)	AZO	576	9.5	32.8	1.8
R7_TT3	$(NH_4)_2S$	CdS	i-ZnO/ITO	336	9.3	33.7	1.1
	KCN	CdS	i-ZnO/AZO	544	12.0	41.3	2.7

2.3. Characterization techniques

The chemical composition was measured by energy dispersive X-ray spectroscopy (EDX) (Oxford instruments, model INCAx-sight) inside a Hitachi S-3000N scanning electron microscope (SEM). EDX measurements were carried out at 25 kV operating voltage, and the Cu-K, Zn-K, Ge-K, Sn-L and S-K lines were used for quantification. Grazing incidence X-ray diffraction (GIXRD) was performed to investigate the structural properties of the CZTS thin films. GIXRD data were collected with a PANAlytical X´Pert Pro MPD diffractometer, using CuK_α radiation and a multilayer mirror to produce a parallel beam. Detector scans with grazing incident angles (GI) of 0.5º, 1º and 3º were carried out. Glow discharge optical emission spectroscopy (GDOES) with a Spectruma GDA 650 was performed in pulsed RF mode to study the elemental profile through the whole CdS/CZTS/Mo layer. Argon plasma with a pulsed RF mode was used to sputter the CdS, CZTS and Mo layer and the ionized atoms from the layer are detected with a CCD array. Micro-Raman spectra were obtained at 21º C in a Horiba Jobin Ivon T64000 spectrometer. The laser wavelength was adjusted to 633 nm and 325 nm with a spot size of 1.25 μm diameter.
I-V characteristics were measured using a Sun 3000 class solar simulator (Abet Technologies Inc., Milford, Connecticut, USA). Measurements were carried out at 25º C and under air mass AM1.5 with 100 mW/cm^2 illumination. External quantum efficiency (EQE) and internal (IQE) measurements were performed using a Bentham PVE300 system (Bentham Instruments Ltd., Berkshire, UK) calibrated with a Si and Ge photodiode. Reversed voltage-biased EQE curves were collected by connecting a Keithley 2400 source meter (Keithley Instruments Inc., Cleveland, Ohio, USA) directly to the primary coil of the transformer and biasing the device at the desired voltage.

3. Results and discussion

The composition of the CZTS thin film summarized in Table 1 shows an increased Cu concentration after evaporation of the precursor compound. At the same time a decreased Zn and Sn content are observed. Figure 1 shows the GIXRD (GI = 1º and 3º) patterns for the as-evaporated sample. Here we find that in addition to CZTS, additional secondary phases corresponding to Cu_2S, ZnS and SnS are identified in the deposited layer. JCPDS data for tetragonal Cu_2ZnSnS_4 (No. 01-075-4122), hexagonal wurtzite ZnS (No. 00-012-0688), cubic Cu_2S (No. 00-053-0522) and orthorrombic SnS (No. 00-039-0354) have been used for identification of the different phases. It is clearly visible, that the Bragg peaks of the secondary phase SnS show an increased intensity at the higher incident angle. This fact indicates that SnS is strongly located deeper in the bulk of the absorber layer, as has been observed for other evaporation techniques [16].

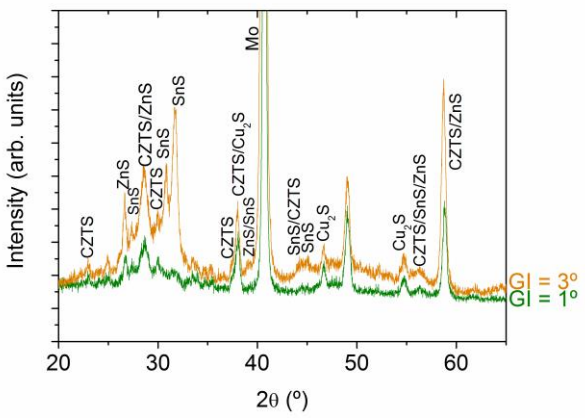

Figure 1. GIXRD spectra of as-evaporated thin films using a GI angle of 1º and 3º.

Following the thermal treatments with variations in the heating rate – 2 ºC/min, 5 ºC/min and 10 ºC/min – GIXRD (GI = 1º) spectra were obtained, shown in Figure 2.a. Variations in the GIXRD spectra were identified for the various heating rates. Cu_2S secondary phase is eliminated with the thermal treatment, lowering the Cu concentration of the annealed-CZTS thin films (see Table 1). However, in all of them, tetragonal CZTS and SnS are identified. In Figure 2.a. is shown a higher intensity of the 111 Bragg peak of SnS for samples annealed at higher heating rates.

GIXRD measurements using different GI angles of 0.5º, 1º and 3º were carried out to investigate the presence of SnS through the absorber layer annealed at the lower heating rate of 2º C/min (see Figure 2.b). A much higher intensity of the Bragg peaks corresponding to SnS are again observed when GI angle is increased. 120, 021, 101, 131 and 211 SnS diffraction peaks are only detected for GI = 3º. Therefore, despite the thermal treatment, significant SnS is still present throughout the depth of the absorber layer.

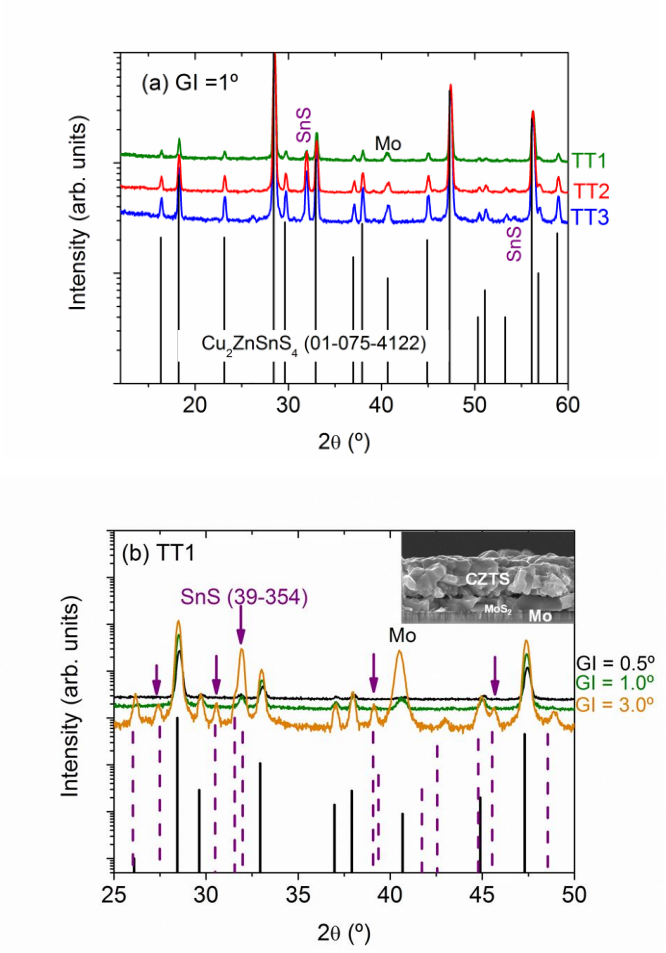

Figure 2. GIXRD spectra of the annealed CZTS thin films (a) following the thermal treatments TT1, TT2 and TT3. (b) GIXRD spectra using the 2º C/min absorber (TT1 treatment) for different GI angles. In (b) the cross-sectional SEM image of the CZTS/Mo/glass structure is displayed.

GDOES measurements of the CdS/CZTS/Mo/glass structure were performed to investigate the influence of the heating rate during the thermal treatment on the elemental distribution. KCN etching was carried out before CdS deposition. Figure 3 shows the GDOES depth profiles for the samples annealed under TT1 and TT3

treatments. Sn is preferentially segregated at the back interface in all cases. A higher Sn concentration next to the Mo back contact is detected for the absorber annealed at the higher heating rate. Additionally, an increased content of S is measured next to the Mo coinciding with the increased Sn concentration. A decrease in Cu and Zn content are also observed at the absorber/Mo back interface. This behavior agrees with the XRD analysis which indicates the preferential formation of SnS towards the back of the absorber. GDOES profiling also indicates Na diffusion from the soda-lime glass into the absorber layer. The positive effect of Na on solar cell performance and the affinity of Na for Cu vacancies is well known for the CIGSe material system [17]. A higher Na concentration near the back contact coincides with the decreased Cu and increased Sn GDOES signals, especially for the sample with 10 ºC/min heating rate. Generally, Na diffuses from the glass towards the absorber surface; however, here an increased Na signal is observed near the front half of the CZTS layer in all cases.

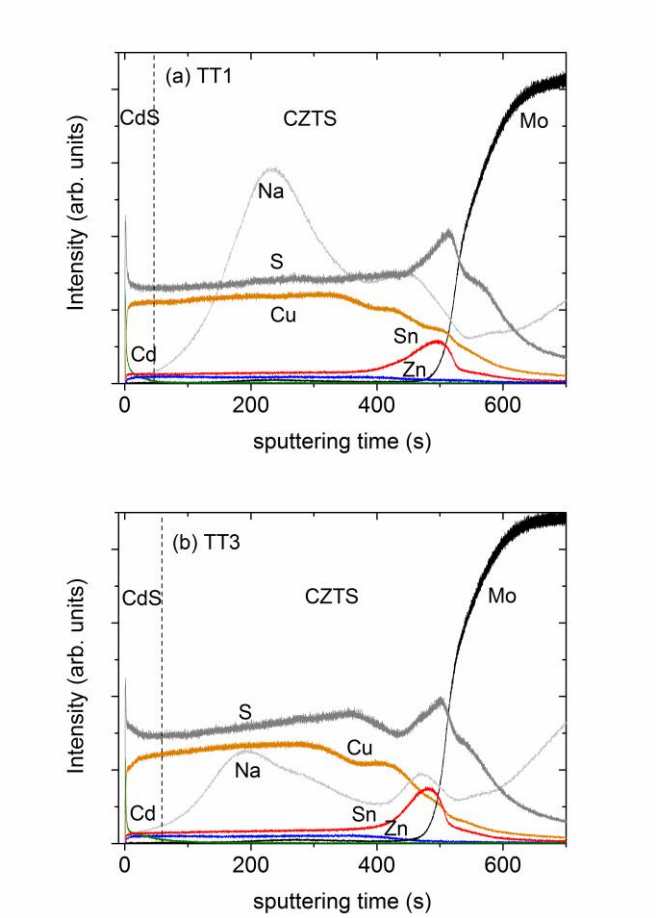

Figure 3. GDOES depth profile of CdS/CZTS/Mo structure for CZTS films annealed following the thermal treatment (a) TT1 and (b) TT3.

Solar cells were fabricated using the absorber thin films of Figure 2. These devices were fabricated with the i-ZnO/In_2O_3:SnO_2 window layer, as described in section 2.2. The corresponding photovoltaic parameters are summarized in Table 2. Here we find the solar cell with the absorber grown with the 2 ºC/min heating rate (TT1) exhibit substantially increased V_{oc} and FF, leading to a higher efficiency of 2.2 %. As observed by GIXRD and GDOES measurements, the presence of SnS in the bulk of the absorber layer and the high content of Sn at the back interface, despite the $(NH_4)_2S$ etching, may be responsible for the low device performance. Chemical etching with $(NH_4)_2S$ is

generally used to remove the SnS secondary phase [7], however it is only effective on the absorber surface. Fernandes et al. [18] have also reported the presence of Sn_xS_y at the back contact. The lower band gap SnS phase next to the Mo layer may result in enhanced recombination of charge carriers near the back contact [19], reducing the short circuit current.

But a question arises now, when and how this SnS secondary phase was formed. A high partial pressure of S during the thermal treatment will cause diffusion of S atoms through the CZTS layer, which will promote the MoS_2 growth. Figure 2.b. shows the cross-sectional SEM micrograph of the absorber layer annealed following the thermal treatment TT1, where a MoS_2 layer of 80 nm thickness can be distinguished at the back interface. Scragg et al. [19] have reported that the presence of MoS_2 and SnS at the back contact is a sign of S transfer across the CZTS/Mo interface. They observed a reaction between the CZTS and Mo during the thermal processing, resulting in decomposition of the CZTS layer into Cu_2S, ZnS and SnS and growth of MoS_2. It is difficult to rule out the presence of Cu_2S and ZnS secondary phases by XRD measurements due to the proximity of the diffraction peaks of these phases with those of CZTS. However, GDOES profiles indicate a decreased signal from Cu and Zn at the back surface. As shown in Figure 1, the as-evaporated sample was composed by Cu_2S, ZnS and SnS secondary phases. The reaction that took place during the annealing follows:

$$2Cu_2S + 2ZnS + 2SnS + S_2 \rightarrow 2Cu_2ZnSnS_4 \quad (1)$$

The loss of Sn when annealing CZTS thin films at high temperatures due to the high partial pressure of SnS has been reported [20]. As shown in Table 1, the Sn excess of the as-evaporated sample was not lost during the annealing treatment. Therefore, the presence of SnS next to the back contact could be explained by the initial formation of SnS during the evaporation of CZTS thin films, in agreement with X-ray diffraction measurements (see Figure 1).

Solar cell devices with the CZTS absorber layers sulfurized at higher heating rates were also fabricated with both the i-ZnO/ITO and i-ZnO/AZO window layer configurations. As shown in Table 2, a higher efficiency of 2.7 % (total area = 0.5 cm^2) (2.9 % for active area) is achieved for the i-ZnO/AZO structure. A higher short circuit current density J_{sc} and fill factor FF are responsible of the higher performance in comparison to the solar cell fabricated using i-ZnO/ITO and 2 ºC/min heating rate. The best pure CZTS device reported up to date achieves an efficiency of 9.1 % with V_{oc} = 0.701 V, J_{sc} = 20.64 mA/cm^2 and FF = 62.5 % [10].

Figure 4.a. shows the EQE spectrum of the best CZTS solar cell fabricated in this study. The EQE is higher than 60 % in the spectral region from 515 to 580 nm. The decline of the EQE in the range from 400 to 515 nm is caused by optical absorption of the CdS buffer layer. A short circuit current density of 12.8 mA/cm^2 is determined from EQE. The optical band gap energy obtained from EQE measurements is 1.63 eV. Internal quantum efficiency (IQE) was also determined by the reflectance measurements of the solar cell. An increased spectral response in the whole range of wavelengths (see figure 4.a.) is observed. A J_{sc} = 14.2 mA/cm^2 is obtained from IQE measurements. This result suggests that the use of an antireflection coating could make possible to enhance the device performance up to 3.2% (active area). However, this J_{sc} value is still very low in comparison with that of the best pure CZTS device reported, and could be related to the presence of SnS phase at the back interface. When comparing reverse-biased EQE

measurement with the EQE without bias (see Figure 4.a.), the solar cell shows an increase in collection for the long wavelengths with negative bias (-1 V). In reverse bias, the depletion width increases and results in improved collection of electrons deeper in the bulk of the CZTS. Such behavior is usually explained by poor collection toward the back of the absorber layer [21]. This fact can be related to the SnS secondary phase detected next to the Mo layer. In order to assure that this SnS secondary phase is not on the absorber surface, Raman measurement was performed on this device. An excitation wavelength of 633 nm was used to avoid the Raman modes of CdS, estimating the penetration depth around 170 nm. As displayed in figure 5.a., only the characteristic Raman peaks of CZTS were detected [22]. In addition to that, the Raman spectra of the absorber layer grown using the thermal treatment TT3 measured with a 325 nm excitation wavelength show the contributions at 347 cm^{-1}, 695 cm^{-1} and 1045 cm^{-1} (see Figure 5.b.). These contributions have been identified with the main vibrational mode of ZnS [23-24] and their second and third order [13, 24-25] respectively. The detection of second and third order is due to the existence of resonant excitation conditions for the ZnS phase. This resonant condition allows for the detection of ZnS phase at extremely low concentrations on the CZTS surface [26]. The main peaks of CZTS are also present in the Raman spectra measured at 325 nm, indicating the low content of ZnS on the surface of the absorber layer [13, 26]. The presence of ZnS on the absorber layer can be another reason for the low device efficiency, reducing the J_{sc} and series resistance [6]. It is possible to remove superficial ZnS secondary phases by HCl-based etching [25]. However, we believe that the SnS secondary phase formed at the back interface plays a more detrimental role that limits the solar cell performance.

As mentioned above, one of the explanations that could explain the low V_{oc} of the kesterite photovoltaic devices is an unfavorable alignment at the CZTS/CdS interface. Here a first experiment was carried out by depositing a Zn(O,S) alternative buffer layers on the absorber layer annealed using TT2. Raman spectroscopy using a 633 nm excitation wavelength was also carried out for this device, detecting only CZTS. Photovoltaic parameters of that device are shown in Table 2. This solar cell presents the highest V_{oc} of 576 mV of the samples investigated here. Ericson et al. [27] reported a V_{oc} of 598 mV for Zn(O,S) deposited by atomic layer deposition on CZTS thin films. Further experiments and investigations are necessary on our samples to determine the origin of this improvement. Figure 4.b. displays the EQE curve of the device with the structure glass/Mo/CZTS/Zn(O,S)/AZO/Ni:Al grids.

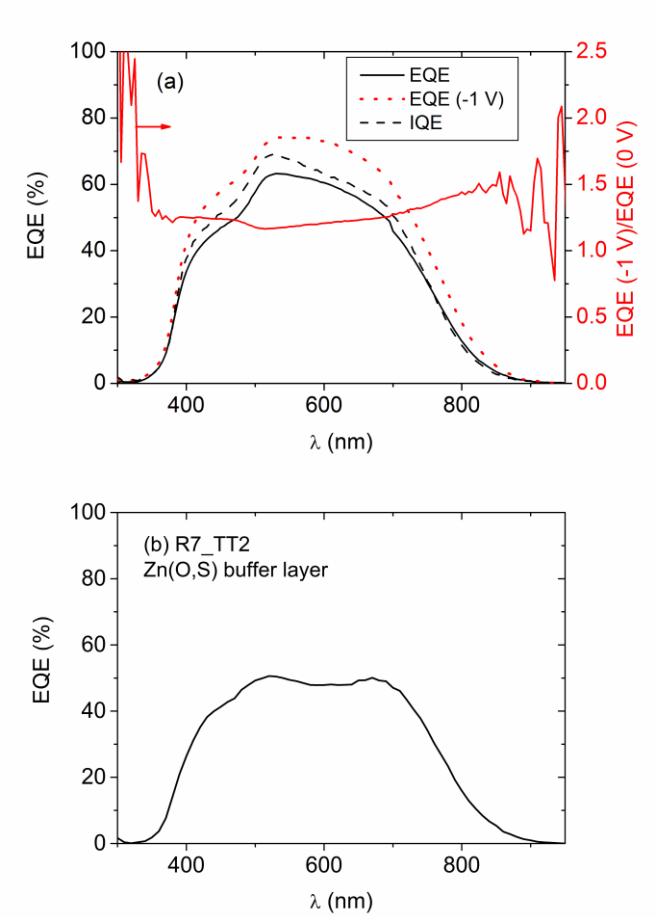

Figure 4. (a) Unbiased EQE, IQE curves and the ratio between voltage biased (-1 V) and unbiased EQE for device structure of AZO/ZnO/CdS/CZTS/Mo (R7_TT3). (b) Unbiased EQE curve for solar cell structure of AZO/Zn(O,S)/CZTS/Mo (R7_TT2).

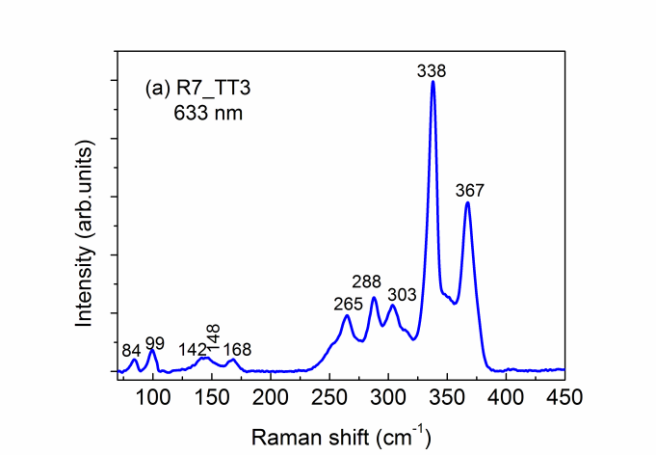

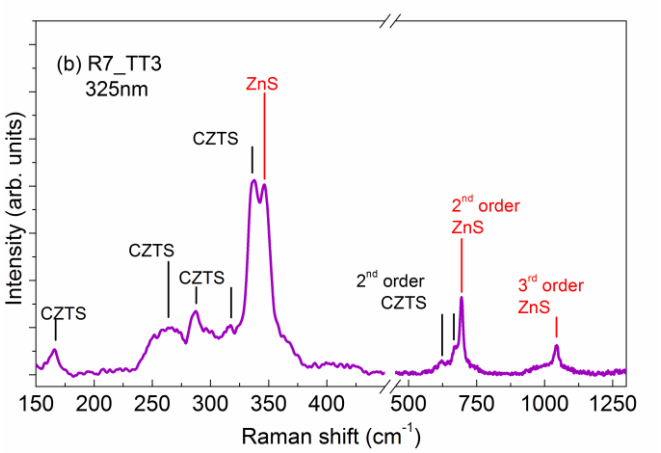

Figure 5. Raman spectroscopy of CZTS thin films annealed using the thermal treatment TT3 measured with (a) 633 nm and (b) 325 nm excitation wavelengths.

4. Conclusions

For the first time, efficiencies in the range of 2-3 % are achieved for CZTS solar cells fabricated by a rapid thermal evaporation of Cu-rich kesterite powder followed by annealing under Ar atmosphere. The influence of the heating rate during the thermal treatment was investigated. Results indicate that a slower heating rate leads to better interdiffusion of the elements; however not sufficient to form a single phase kesterite material. The presence of SnS secondary phase near the Mo back contact formed during the evaporation is the main reason of the limited device performance. A first attempt to increase the V_{oc} of the solar cells via the use of a Zn(O,S) buffer layer was carried out successfully.

Acknowledgments

This work was supported by DAAD project (INTERKEST, Ref: 57050358), Marie Curie-ITN (KESTCELLS, GA: 316488) and MINECO project (SUNBEAM, ENE2013-49136-C4-3-R). RC and ES acknowledge financial support from Spanish MINECO within the Ramón y Cajal program (RYC-2011-08521) and (RYC-2011-09212) respectively. SG also thanks the Government of Spain for the FPI fellowship (BES-2014-068533). The authors would also like to thank C. J. Hages for English revision.

References

[1] Mitzi, D.B., Gunawan, O., Todorov, T.K., Wang, K., Guha, S., 2011. The path towards a high-performance solution-processed kesterite solar cell. Sol. Energy Mater. Sol. Cells. 95, 1421-1436.

[2] Wang, W., Winkler, M.T., Gunawan, O., Gokmen, T., Todorov, T.K., Zhu, Y., Mitzi, D.B., 2014. Device characteristics of CZTSSe thin-film solar cells with 12.6% efficiency. Advanced Energy Materials. 4, 1301465.

[3] http://www.pv-magazine.com/news/details/beitrag/zsw-sets-new-thin-film-solar-world-record-with-226-efficient-cigs-pv-cell_100024995/#axzz4OrbqyhKf. 15 June 2016.
[4] Liu, X., Feng, Y., Cui, H., Liu, F., Hao, X., Conibeer, G., Mitzi, D.B., Green, M., 2016. The current status and future prospects of kesterite solar cells: a bried review, Progr. Photovolt.: Res. Appl. 24, 879-898.
[5] Plätzer-Björkman, C., Frisk, C., Larsen, J.K., Ericson, T., Li, S.Y., Scragg, J.S., Keller, J., Larsoon, F., Törndahl, T., 2015. Reduced interface recombination in Cu_2ZnSnS_4 solar cells with atomic layer deposition $Zn_{1-x}Sn_xO_y$ buffer layers. Appl. Phys. Lett. 107, 243904.
[6] Siebentritt, S., Schorr, S., 2012. Kesterites- a challenging material for solar cells. Prog. Photov: Res. Appl. 20, 512-519.
[7] Xie, H.; Sánchez, Y.; López-Marino, S.; Espíndola-Rodríguez, M.; Neuschitzer, M.; Sylla, D.; Fairbrother, A.; Izquierdo-Roca, V.; Pérez-Rodríguez, A.; Saucedo, E., 2014. Impact of Sn(S,Se) Secondary Phases in $Cu_2ZnSn(S,Se)_4$ Solar Cells: a Chemical Route for Their Selective Removal and Absorber Surface Passivation. ACS Appl. Mater. Interfaces. 6, 12744-12751.
[8] Fairbrother, A., Dimitrievska, M., Sánchez, Y., Izquierdo-Roca, V., Pérez-Rodríguez, A., Saucedo, E., 2015. J. Mater. Chem. A 3, 9451.
[9] Scragg, J., Larsen, J., Kumar, M., Persson, C., Sendler, J., Siebentritt, S., Plätzer-Björkman, C., 2016. Cu-Zn disorder and bandgap fluctuations in $Cu_2ZnSn(S,Se)_4$: Theoretical and experimental investigations, Phys. Status Solidi B. 253, 247-254.
[10] Tajima, S., Asahi, R., Isheim, D., Seidman, D.N., Itoh, T., Hasegawa, M., Ohishi, K., 2014. Atom-probe tomographic study of interfaces of Cu_2ZnSnS_4 photovoltaic cells, Citation: Appl. Phys. Lett. 105, 093901.
[11] Fukano, T., Tajima, S., Ito, T., 2013. Enhancement of Conversion Efficiency of Cu_2ZnSnS_4 thin film solar cells by improvement of sulfurization conditions. Appl. Phys. Express. 6, 062301.
[12] Valle-Rios, L.E., Neldner, K., Gurieva, G., Schorr, S., 2016. Existence of off-stoichiometric single phase kesterite, Journal of Alloys and Compounds. 657, 408 – 413.
[13] Caballero, R., Cano-Torres, J.M., Garcia-Llamas, E., Fontané, X., Pérez-Rodríguez, A., Greiner, D., Kaufmann, C.A., Merino, J.M., Victorov, I., Baraldi, G., Valakh, M., Bodnar, I., Izquierdo-Roca, V., León, M., 2015. Towards the growth of $Cu_2ZnSn_{1-x}Ge_xS_4$ thin films by a single-stage process: Effect of substrate temperature and composition. Sol. Energy Mater. Sol. Cells 139, 1-9.
[14] Lehmann, J., Lehmann, S., Lauermann, I., Rissom, T., Kaufmann, C.A., Lux-Steiner, M.Ch., Sadewasser, S., 2014. Reliable wet-chemical cleaning of natively oxided high-efficiency $Cu(In,Ga)Se_2$ thin film solar cell absorbers. J. Appl. Phys. 116, 233502.
[15] Klenk, R., Steigert, A., Rissom, T., Greiner, D., Kaufmann, C.A., Unold, T., Lux-Steiner, M.Ch., 2014. Junction formation by Zn(O,SO sputtering yields CIGSe-based cells with efficiencies exceeding 18%. Progr. Photovolt.: Res. Appl. 22, 161-165.
[16] Fairbrother, A., Fontane, X., Izquierdo-Roca, V., Espindola-Rodriguez, M., López, S., Placidi, M., Calvo-Barrio, L., Perez-Rodriguez, A., Saucedo, E., 2013. On the formation mechanisms of Zn-rich Cu_2ZnSnS_4 films prepared by sulfurization of metallic stacks, Sol. Energy Mater. Sol. Cells. 112, 97-105.
[17] Caballero, R., Kaufmann, C.A., Efimova, V., Rissom, T., Hoffmann, V., Schock, H.W., 2013. Investigation of $Cu(In,Ga)Se_2$ thin-film formation during the multi-stage coevaporation process. Prog. Photovolt. Res. Appl. 21, 30-46.

[18] Fenandes, P.A., Salomé, P.M.P., da Cunha, A.F., 2011. Study of polycrystalline Cu_2ZnSnS_4 films by Raman scattering. J. Alloys and Compounds. 509, 7600.
[19] Scragg J.J., Wätjen, J.T., Edoff, M., Ericson, T., Kubart, T., Platzer-Björkman, C., 2012. A detrimental reaction at the molybdenum back contact in $Cu_2ZnSn(S,Se)_4$ thin-film solar cells. J. Am. Chem. Soc. 134, 19330-19333.
[20] Weber, A., Mainz, R., Schock, H.W., 2010. On the Sn loss from thin films of the material system Cu–Zn–Sn–S in high vacuum, J. Appl. Phys. 107, 013516 (5 pages).
[21] Scheer, R., Schock, H.W., Chalcogenide Photovoltaics, Weinheim, Germany; Wiley-VCH Verlag, 2011.
[22] Dimitrievska, M., Fairbrother, A., Fontané, X., Jawhari, T., Izquierdo-Roca, V., Saucedo, E., Pérez-Rodríguez, A., 2014. Appl. Phys. Lett. 104, 021901.
[23] Schneider, J., Kirby, R.D., 1972. Raman scattering from ZnS polytypes, Phys. Rev. B 6, 1290-1294.
[24] Fontané, X., Calvo-Barrio, L. , Izquierdo-Roca, V., Saucedo, E., Pérez-Rodriguez, A., Morante, J. R., Berg, D. M., Dale, P. J., Siebentritt, S., 2011. In-depth resolved Raman scattering analysis for the identification of secondary phases: Characterization of Cu_2ZnSnS_4 layers for solar cell applications, Appl. Phys. Let. 98, 181905.
[25] Fairbrother, A., García-hemme, E., Izquierdo-Roca, V., Fontané, X., Pulgarín-Agudelo, F.A., Vigil-Galán, O., Pérez-Rodríguez, A., Saucedo, E., 2012. Development of a selective chemical etch to improve the conversion efficiency of Cu_2ZnSnS_4 solar cells, J. Am. Chem. Soc. 134, 8018-8021.
[26] Fairbrother, A., Izquierdo-Roca, V., Fontané, X., Ibáñez, M., Cabot, A., Saucedo, E., Pérez-Rodríguez, A., 2014. ZnS grain size effects on near-resonant Raman scattering: optical non-destructive grain size estimation. Cryst. Eng. Comm 16, 4120-4125.
[27] Ericson, T., Scragg, J.J., Hultqvist, A., Wätjen, J.T., Szaniawski, P., Törndahl, T., Platzer-Björkman, C., 2014. Zn(O,S) buffer layers and thickness variations of CdS buffer for Cu_2ZnSnS_4 solar cells. IEEE Journal of Photovoltaics 4, 465-469.